*Materials Science-Poland, Vol. 25, No. 2, 2007*

# Image processing study of ultrathin cobalt domain structure evolution induced by overlayer structure

W. DOBROGOWSKI[1], Z. KURANT[1, 2], A. NEDZVED[1, 3], W. STEFANOWICZ[1*], M. TEKIELAK[1], L.T. BACZEWSKI[2], A. WAWRO[2], A. MAZIEWSKI[1]

[1]Institute of Experimental Physics, University of Białystok, Lipowa 41, 15-424 Białystok, Poland

[2]Institute of Physics, Polish Academy of Sciences, al. Lotników 32/46, 02-668 Warsaw, Poland

[3]United Institute of Informatics Problems, National Academy of Sciences BY-220012 Minsk, Belarus

Evolution of the domain structure (DS) in ultrathin cobalt films, deposited on sapphire substrate with the following structure: X\Au\Co($d_{Co}$ nm thick layer or wedge)\X ($d_X$ nm thick layer or wedge perpendicular to Co wedge axis)\Au (where X is V or Mo) with perpendicular magnetization was investigated as a function of thickness $d_X$. The study was performed using an optical polarizing microscope with CCD camera. Images of DS were recorded during various stages of magnetization reversal. A special software based on LabView® was employed for acquisition and processing of domain images. To analyze the observed domain structures, topology properties of magnetic images were determined. Preferential orientation of domain walls was found in ultrathin Co covered by Mo but not by V.

Key words: *magnetic domains; ultrathin film; cobalt*

## 1. Introduction

Magnetic ordering of ultrathin films is one of the intensively studied phenomena. Magnetic reorientation phase transition (RPT) in sandwich structures containing ultrathin Co films between vertical and in-plane magnetization states attracts particular attention of scientists all over the world. RPT can be induced by changing: (i) thickness $d$ of the magnetic layer or (ii) overlayer and/or underlayer structures [1, 2]. Changes of magnetic domain structure (DS) in ultrathin Co, approaching RPT have been studied *in-situ* by the SEMPA technique [3] which showed a decrease of DS size, and *ex-situ* by magnetooptical microscopy [4, 5] during which an increase of the density of magnetization reversal nucleation centres and an appearance of dendrite

*Corresponding author e-mail: vstef@uwb.edu.pl

type DSs were observed. In the present work, the influence of V and Mo overlayers on DS geometry near RPT is investigated in detail. An image processing technique was developed for this purpose.

The results were obtained on two selected MBE-grown epitaxial samples, deposited on monocrystalline (11–20) $Al_2O_3$ substrate, with the following structures: (i) V (20 nm)\Au(111) (20 nm)\Co (6 mm long wedge; 1 nm < $d$ <1.5 nm)\V(6 mm long wedge; 0 < $d_V$ < 0.3 nm perpendicular to the Co one)\Au (8 nm) and (ii) Mo(110) (20 nm)\Au(111) (20 nm)\Co ($d$ =1.2 nm)\Mo ($d_{Mo}$= 0.15 nm)\Au(8 nm).

All measurements, based on the polar Kerr effect, were performed at room temperature using a classical optical polarizing microscope with a CCD camera. Perpendicular to the sample plane, magnetic field pulses or alternating field $H_{AC}$ with decreasing amplitude was applied after saturation to induce the domain structure. A DS image was recorded after different magnetic histories (Fig. 1). To improve the image contrast, the following normalization numerical procedure was used:

$$P(i, j) = (I_+(i, j) - I_-(i, j))/(I_+(i, j)+I_-(i, j)) \tag{1}$$

where $I_-$ denotes the level in the grey scale of an individual image pixel positioned at ($i$, $j$) of the reference image recorded in remnant state after sample saturation at $H_S < 0$ and $I_+$ describes the pixel value after application of the pulse of magnetic static field with the amplitude $H_+$ or $H_{DS}$ in the opposite direction ($I_+$ or $I_D$) or AC field with decreasing amplitude. The gray level of the pixels is proportional to the local values of both the normalized remnant magnetization $m_R$ and maximal Kerr rotation $\varphi_{max}$.

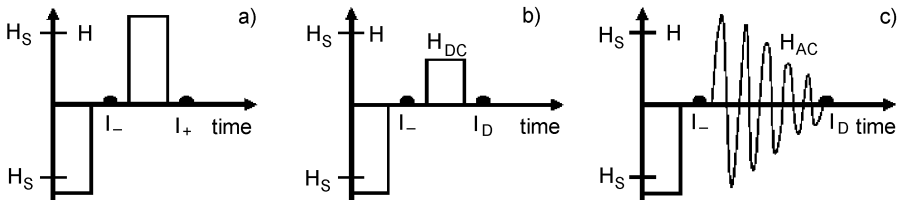


Fig. 1. Various procedures of domain structure imaging

We assume that each image sample element $P$ ($i$, $j$) consists of two components: a constant nonmagnetic component presented in all images and a magnetooptical component detected in images with multidomain structure. Considering a constant component as a background of the image, the standard operation of background correction of image improvement [6, 7] is applied:

$$C_{i,j} = \frac{\left(P_{i,j} - B_{i,j}\right)\left(W_{\max} - B_{i,j}\right)}{\left(W_{i,j} - B_{i,j}\right)} \tag{2}$$

where $Pi, j$ is the value of the pixel brightness in the image with magnetooptical component, $B_{i,j}$ – the value of the pixel in an image without a magnetooptical component,

$W_{i,j}$ – the value of the pixel of the image at full CCD saturation of the chamber (light overflow), $W_{\max}$ is the maximum value of brightness of the image at saturation of chamber and $C_{i,j}$ is a new value of the pixel brightness in the corrected image.

We reduced shot noise by applying the median filter. The median filter is a nonlinear lowpass filter which replaces the gray scale value of each pixel by the median grayscale value of the pixel and of its 24 neighbours. This procedure effectively removes shot noise but leaves dendrites, which typically have an effective width covering many pixels.

Let us first describe properties of a double wedge sample with vanadium coverage. Figure 2 illustrates the remnant magnetic state of the sample. Domain structure images recorded in A and B regions marked in Fig. 2, are shown in the first and second row in Fig. 3, respectively. Domain structures were obtained using two following procedures: (i) ac demagnetization (see the scheme in Fig. 1c) after applying alternating field with decreasing amplitude; exemplary images are shown in the first column in Fig. 3; (ii) direct magnetization reversal process [8] (scheme of the procedure in Fig. 1b); images are shown in the second column in Fig. 3. For detection of geometrical characteristics it is necessary to take a binary image. Image binarisation is executed by thresholding using Otsu method [9].

Next we measure such parameters of the domain structure as the area, perimeter, the linear sizes, and shape factor. Because of the digital character of the image there are two ways of calculation of geometrical characteristics: traditional and planimetric. In both of these methods every pixel has a linear size, and calculation of geometrical characteristics is carried out on a selected point. In the traditional method, this point is in the centre of the pixel and the size is equal to the area of pixel. The planimetric calculations operate with the linear distances between points placed in the corners of the pixel. Thus, in planimetric calculations the vertical and horizontal distances between points are equal to the linear sizes of a pixel, but diagonal distances are defined by Pythagorean theorem. The perimeter is calculated in similar terms as a contour of object.

For determination of topological parameters of the image, the binarisation of images was done as in the previous case. Topological characteristics are allocated by means of the Boolean logic operations for images and mathematical morphology smoothing. We defined three topological regions in dendrite images: body of dendrites, fiords and holes (Fig. 3 AIII, BIII). Fiords and holes are the regions between dendrites. Fiords are connected with free space. Holes are enclosed only by white body of dendrites. For the description of these topology features, we propose the following characteristics: total area, fiord ratio, hole ratio, dendrite ratio. The total area is defined as a sum of all topological region areas. Other characteristics corresponding to space filling are defined by relations between areas of particular regions and total area. For description of other topological properties of dendrites, it is necessary to extract the dendrite skeleton from a binary image. This operation is realized by the binary thinning operation (Zang–Suen algorithm [10]). The basic objects used for the calculations are body, skeleton, nodes and tails (Fig. 4), where body corresponds to

the region of white domain; skeleton is the mean line of dendrites; nodes are the points of dendrite branching, segments are the branches between two nodes and tails are the "last branches" of dendrites. To describe the topology features of a dendrite, we define the following characteristics: dendrite length, mean dendrite width, tailness, tail curliness, tails ratio. The dendrite length corresponds to the length of the skeleton. The tailness and tails curliness are defined as count of tails per skeleton length unit and the ratio between the count of tails and the count of segments and the last parameter – tails ratio is the ratio between length of tails and length of skeleton.

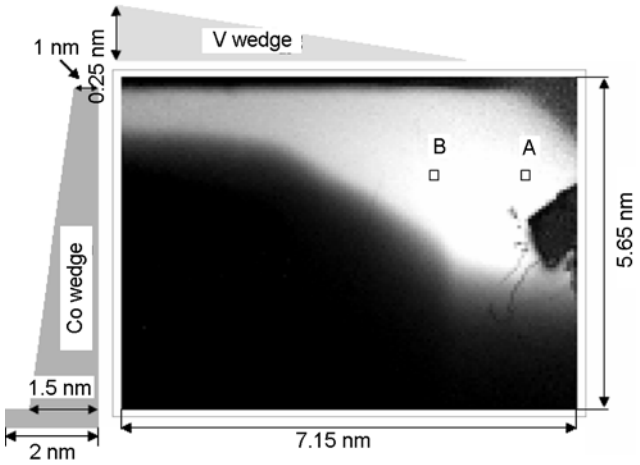


Fig. 2. Remnant magnetization state of the sample with vanadium overlayer

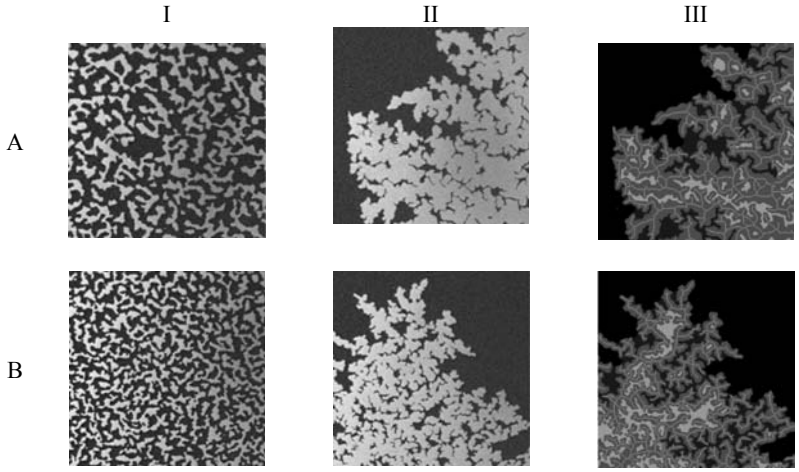


Fig. 3. Domain structures in V-covered sample. The images from the first and the second row were recorded in the A and B areas marked with squares in Fig. 2. Images in the columns were obtained by: (i) ac procedure after applying alternating field (first column); (ii) direct magnetization reversal process (see Fig. 1b) applying DC field pulse to initially saturated sample (second column); (iii) processing of images from the second column (third column). Images size is 100×100 $\mu m^2$

Dendrite width is a more complicated characteristic because it changes from point to point. Moreover, it is impossible to define skeleton width in points corresponding to the nodes and dendrite crossings. Points of skeleton ends distinguish from noise points in a very complex way. To solve these problems, we approximate the mean dendrite width by a relation between the area of dendrites and the length of a skeleton.

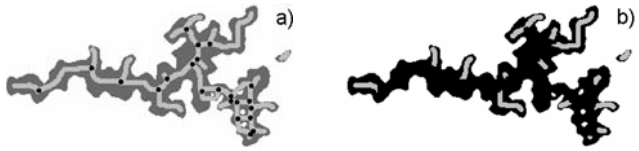


Fig. 4. Topological parameters of dendrites: a) gray – dendrite body, light gray – skeleton, black – nodes; b) black – dendrite body, gray – tails

The last characteristic of the domain structure that is necessary to introduce is the dendrite orientation. The orientation diagram (see insets in Fig. 5) illustrates the dependence of segment length on direction (the angle between line containing segment and horizontal line in the image). The preference of DS direction may be connected with in-plane anisotropy introduced by the molybdenum overlayer.

Table 1. Topological parameters of DS images

| Image | Total area [μm$^2$] | Fiord ratio | Hole ratio | Dendrite ratio | Dendrite length [μm] | Mean dendrite width [μm] | Tailness [μm$^{-1}$] | Tail curliness | Tail ratio |
|---|---|---|---|---|---|---|---|---|---|
| A | 6970 | 0.16 | 0.09 | 0.75 | 1405 | 4.96 | 0.11 | 0.37 | 0.33 |
| B | 5970 | 0.18 | 0.12 | 0.70 | 1484 | 4.02 | 0.15 | 0.50 | 0.39 |

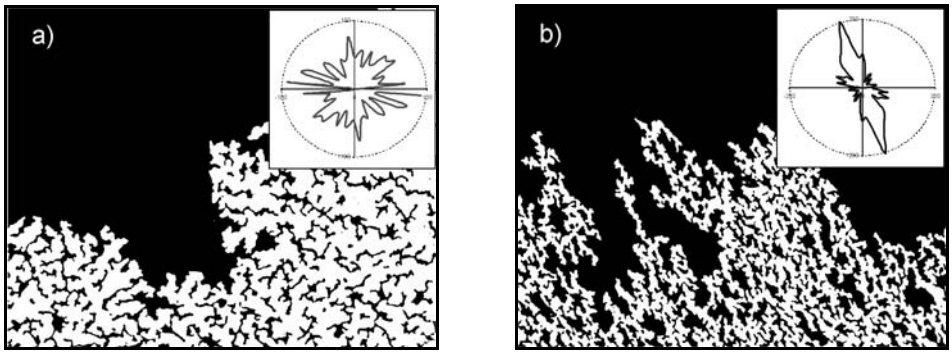


Fig. 5. Domain structure images of sample with: a) vanadium (effective $d_V$ = 0.03 nm), b) molybdenum overlayer. Insets illustrate orientation of dendrites

The values of the parameters described above are given in Table 1. Comparing images in Fig. 3 one can mention that the size of domains decreases with approaching RPT, the mean width of dendrites also decreases, and such parameters as tailness, tail

curliness etc. also change. Mo induced domain orientation is shown in Fig. 5. The observed preference of DS in Fig. 5 could be related to in-plane magnetic anisotropy which is connected with pseudomorphic growth of Mo overlayer.

## References

[1] HEINRICH B., BLAND J.A.C., *Ultrathin Magnetic Structures*, Springer, Berlin, 1994 and references therein.
[2] KISIELEWSKI M., MAZIEWSKI A., TEKIELAK M., WAWRO A., BACZEWSKI L.T., Phys. Rev. Lett., 89 (2002), 87203 and references therein.
[3] HOPSTER H., OEPEN H.P., *Magnetic microscopy of nanostructures, NanoScience and Technology*, Springer, Berlin, 2005.
[4] KISIELEWSKI M., KURANT Z., TEKIELAK M., DOBROGOWSKI W., MAZIEWSKI A., WAWRO A., BACZEWSKI L.T., Phys. Status Sol. (a), 196 (2003), 129.
[5] STEFANOWICZ W., TEKIELAK M., BUCHA W., MAZIEWSKI A., ZABLOTSKII V., BACZEWSKI L.T., WAWRO A., Mater. Sci.-Poland, 24 (2006), 783.
[6] RITTER G.X., WILSON J.N., *Handbook of Computer Vision Algorithms in Image Algebra*, CRC Press, Boca Raton, Fl, USA, 1996.
[7] PATURI P., HVOLBEK LARSEN B., JACOBSEN B.A., ANDERSEN N.H., Rev. Sci. Instr., 74 (2003), 2999.
[8] FERRE J., GROLIER V., MEYER P., MAZIEWSKI A., STEFANOWICZ E., TARASENKO S.V., TARASENKO V.V., KISIELEWSKI M., RENARD D., Phys. Rev. B, 55 (1997), 15092.
[9] SAHOO P.K., SOLTANI S., WONG A.K.C., CHEN Y.C. Comp. Vision Graph. Image Proc., 41 (1988), 233.
[10] ZHANG T.Y., SUEN C.Y., Comm. ACM, 27 (1984), 236.

*Received 7 May 2006*
*Revised 1 September 2006*